The symmetry of the $F_H(CN^-)$ defect centre in CsBr: a study of polarized resonant anti-Stokes Raman scattering

1992 J. Phys.: Condens. Matter 4 9269

(http://iopscience.iop.org/0953-8984/4/47/009)

J. Phys.: Condens. Matter 4 (1992) 9269–9282. Printed in the UK

The symmetry of the $F_H(CN^-)$ defect centre in CsBr: a study of polarized resonant anti-Stokes Raman scattering

R Albrecht, H Stolz and W von der Osten

Fachbereich Physik, Universität Paderborn, D-4790 Paderborn, Federal Republic of Germany

Received 13 August 1992

Abstract. For the F-centre/CN^- defect complex ('$F_H(CN^-)$ centre') in CsBr, the polarization dependence of anti-Stokes Raman scattering is investigated. Comparison with calculated intensities shows that the results are inconsistent with the suspected C_{4v} point symmetry of this centre. Possible explanations are considered, including structural models with lower symmetry and reorientational effects of the CN^- molecular ion.

1. Introduction

The $F_H(CN^-)$ defect belongs to a recently discovered novel class of aggregate centres in alkali halides in which an F centre (anion vacancy plus trapped electron) is associated with a substitutionally built-in molecular ion (for a survey see, e.g., Rong *et al* 1989). The new and most exciting feature of this defect originates in the molecular character of the associated impurity. Optical excitation of the F_H/CN^- pair in its electronic absorption bands causes a transfer of energy into the vibrational states of the CN^- stretching mode which, depending in detail on the host crystal, become populated up to the $v = 5$ level (v = vibrational quantum number). One way in which this excited population can be probed is by looking for the infrared vibrational fluorescence. It shows up in the 5 μm range and consists of a series of nearly equidistant ($\Delta E = 3.1$ meV or 25 cm^{-1}) lines (Yang *et al* 1985). These correspond to $\Delta v = -1$ transitions shifted due to the small anharmonicity of the vibration. The other technique for monitoring the population of the vibrational states is resonant Raman scattering which, besides the usual Stokes component, exhibits strong anti-Stokes lines due to the highly excited CN^- stretching mode. Both vibrational emission and Stokes/anti-Stokes resonant Raman scattering were recently employed to extensively study the properties of this new type of defect (Cachei *et al* 1989; Rong *et al* 1989).

Concerning the microscopic structure of the $F_H(CN^-)$ centres, one expects the CN^- molecular ion to occupy a next-nearest-neighbour (NNN) lattice site relative to the F centre. Accordingly in KCl and other face-centred cubic alkali halides the $F_H(CN^-)$ pair axis should be oriented along ⟨110⟩ as was actually verified by recent ENDOR measurements (Jordan *et al* 1988). In cesium halides, on the other hand, which have a body-centre cubic crystal structure, the centre axis is assumed to be directed along ⟨100⟩. While magnetic resonance experiments to establish a structural model do not exist, this knowledge came essentially from the polarization behaviour

0953-8984/92/479269+14$07.50

of the infrared vibrational emission observed for polarized excitation in the $F_H(CN^-)$ absorption (Yang *et al* 1985). As illustrated in figure 1, the $F_H(CN^-)$ absorption consists of two separate bands, $F_H(1)$ and $F_H(2)$, which were found to absorb predominantly radiation polarized parallel and perpendicular to the F-centre/CN^- pair axis. This was taken as evidence for the axial symmetry and the structural model with symmetry C_{4v}. In fact the situation was considered largely analogous to the well known F_A centre (which consists of an F centre associated with a NNN alkali ion) where the reduction of F-centre (O_h) symmetry by the associated impurity leads to a splitting of the excited F-centre 2p state and to electronic transition moments parallel and perpendicular to the axis (see, e.g., Lüty 1968). In the case of the $F_H(CN^-)$ defect, where one of the constituents is a molecular rather than an atomic impurity, this is not necessarily the case. In particular, depending on the detailed interaction of the molecular ion with the F-centre electron and also the surrounding lattice ions, the molecular axis may deviate from the hitherto tacitly assumed orientation parallel to the F centre/CN^- pair axis leading to a lower symmetry of the defect. Indications of this were discovered in the magnetic resonance of the $F_H(CN^-)$ centre in KCl already mentioned (Jordan *et al* 1988) which suggested that the CN^- electric dipole moment is not directed towards the F centre, i.e. along the ⟨110⟩ centre axis, but very probably along ⟨111⟩. Also, the deviations in polarized vibrational emission observed for the $F_H(CN^-)$ defect in CsCl as host from the behaviour expected for the C_{4v} structural model, as well as previous Raman results in CsBr, indicate the necessity to refine the model (Yang *et al* 1985, Cachei *et al* 1988).

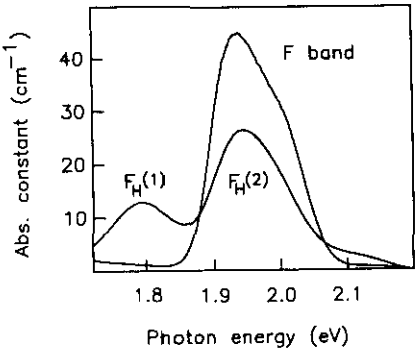

Figure 1. Absorption spectra of F centres and $F_H(CN^-)$ centres in CsBr + 0.5% CsCN at 15 K. The F centres are produced by additive colouration and are subsequently aggregated with the CN^- to form the $F_H(CN^-)$ centres.

In trying to obtain information on the $F_H(CN^-)$ defect structure, we performed detailed investigations of polarized anti-Stokes resonant Raman scattering of this defect in CsBr and compared the results with corresponding predictions for various models.

2. *Experimental details*

The crystals were grown in our crystal growth facility by the Bridgman technique with Merck CsBr Suprapur as starting material and 0.5 mol% CsCN added to the

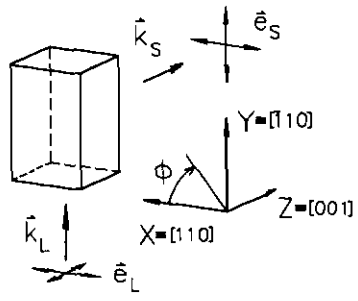

Figure 2. Scattering geometry employed for the polarized Raman measurements. The axes X, Y and Z of the laboratory reference system were always oriented parallel to the crystal directions [110], [$\bar{1}$10] and [001], respectively. The angle ϕ in the X–Y plane defines the direction of polarization of the scattered light, $\boldsymbol{k}_L$, $\boldsymbol{e}_L$ and $\boldsymbol{k}_S$, $\boldsymbol{e}_S$ denote wavevectors and polarization unit vectors of the incident (laser) and the scattered light.

melt. To keep the water content as low as possible, the CsBr powder was dried in high vacuum at 570 K. Using commercially available CsCN, the final grown crystals contained considerable concentrations of various isotopic species of NCO^-. They were recognized by characteristic vibrational absorption bands in the range of 2100–2170 cm^{-1} (260–269 meV) which were much stronger than the (desired) CN^- fundamental absorption. In such samples, $F_H(CN^-)$ centres could not be produced by the usual aggregation process (see below). Therefore the doping material was synthesized according to the reaction $CsOH + HCN \rightarrow CsCN + H_2O$. To reduce the amount of carbonate responsible for the formation of CsCNO (DeLong and Rosenberger 1986), the CsCN powder was distilled several times in vacuum at about 830 K. It thereby transformed into polycrystalline material which was kept in sealed evacuated glass tubes until it was used. The crystals grown with this material essentially exhibited the typical CN^- infrared vibrational absorption without further absorption due to any perturbing molecular species and easily allowed aggregation of the F centre and CN^- ion.

The grown crystals were carefully oriented by means of the Laue technique. They were sawn into pieces of several mm side length with two {100} and four {110} orthogonal faces and coarsely ground. To produce the necessary F centres, the samples were additively coloured in potassium vapour as described previously (Cachei *et al* 1989). Before mounting the coloured samples to the cold finger of a variable-temperature cryostat, they were polished and finally quenched to avoid F-centre aggregation. To produce the F-centre/CN^- pairs, the samples were cooled to 165 K and irradiated for $\sim$ 30 min with F band light from either a dye laser or a halogen lamp equipped with an interference filter. To obtain a homogeneous distribution of $F_H(CN^-)$ defects, the bleaching beams were expanded, and the crystal rotated several times during the (F-centre/CN^-) aggregation process. Following this procedure, the sample was left in the dark for up to 20 min to allow an additionally produced absorption band at 1.61 eV to fade out before it was cooled to the lower temperatures (5–15 K) used for the measurements. Figure 1 illustrates the corresponding absorption spectra showing the F- and double peaked $F_H(CN^-)$ absorption bands prior to and after the aggregation process.

The spectroscopic equipment for the Raman measurements was similar to that

described previously (Cachei *et al* 1989). The scattered light was observed at 90° relative to the incident laser beam as illustrated in figure 2. We adopt and use throughout this paper two sets of reference axes. One is the laboratory system X, Y, Z, relative to which the principal crystal directions are fixed with $X \| [110]$, $Y \| [\bar{1}10]$ and $Z \| [001]$, corresponding to the chosen sample orientation. The wave vectors ($k_{L,S}$) and polarization vectors ($e_{L,S}$) of the incident (laser) and scattered light (subscripts L and S, respectively) will refer to this system. An angle ϕ relative to the X-axis is introduced to define the direction of polarization of the scattered light. In addition, we make use of the crystal reference system with coordinates $X_c \| [100]$, $Y_c \| [010]$ and $Z_c \| [001]$ in which the local symmetry of the defect will be represented.

A major source for systematic errors in measuring the Raman intensities might be deviations in crystal orientation relative to the sample surfaces and the polarization directions. Therefore special care was taken to keep these as small as possible. By allowing deviations in angle of ±5° around the X- or Y-axes, we convinced ourselves that the error in detected intensity is negligible, the acutal crystal misorientations being less than about ±2°.

3. Polarized Raman scattering: experimental data

Anti-Stokes Raman spectra obtained for excitation in resonance with the $F_H(CN^-)$ absorption (figure 1) are displayed in figures 3, 4 and 5. As observed previously in CsBr under similar experimental conditions of excitation power and temperature (Cachei *et al* 1989), their appearance differs significantly depending on laser photon energy. Excitation in the $F_H(1)$ component, in spite of smaller absorption, gives rise to strong scattering with up to six Raman lines, while only three lines are observed for $F_H(2)$ excitation. For the two energies the strength of relative intensities reflect the highest population of the $v = 3$ vibrational level under these conditions.

Employing the scattering geometry of figure 2, we measured the polarization dependence of these spectra for excitation in the two absorption components $F_H(1)$ and $F_H(2)$. The excitation photon energies (at $E_L = 1.775$ eV and 1.980 eV) were chosen slightly below and above each absorption maximum to reduce effects due to possible overlap of the two bands. Figures 3 and 4 show the results obtained with $F_H(1)$ excitation. The directions of polarization of the exciting laser are $e_L \| X$ and $e_L \| Z$, respectively, whereas the scattered light polarization is rotated in steps of 15° or 30° with the directions as given. Corresponding results for $F_H(2)$ excitation and the main directions of polarization are displayed in figure 5.

There are two remarkable observations in figures 3–5 that will be important with regard to the analysis below.

(i) Appreciable intensities do occur under *all* conditions of polarization. In particular, non-negligible Raman signals are detected for $e_L \| Z$ (figures 4, 5) which, as will be demonstrated later, are not to be expected for the C_{4v} model of the $F_H(CN^-)$ centre.

(ii) Considering the series of spectra for $e_L \| X$ in figure 3, the effect of rotation of the analyser on the line intensities is significantly different for each $v \rightarrow v-1$ Raman transition and cannot be expressed by a common factor as one would expect. This becomes directly obvious if one compares the relative strengths of the $v = 2 \rightarrow 1$ and $v = 4 \rightarrow 3$ in X, X-polarization ($\phi \approx 0$) with that in X, Y-polarization ($\phi = 90°$)

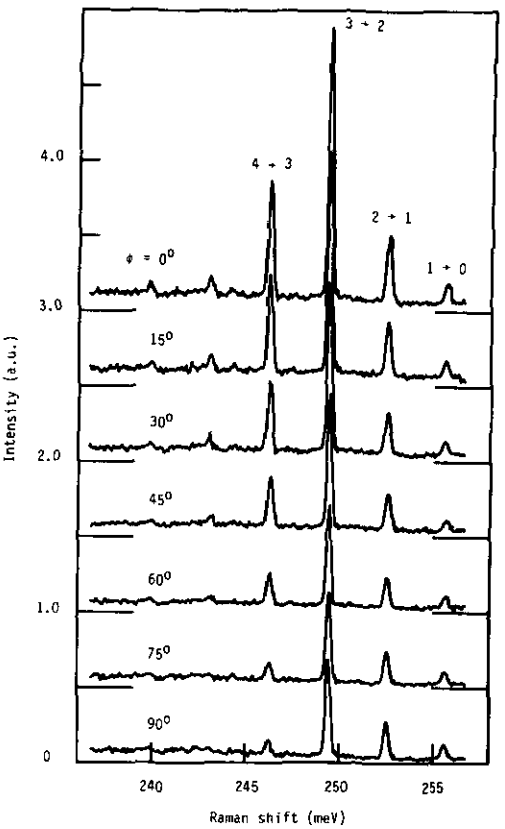

Figure 3. Anti-Stokes resonant Raman spectra excited in the $F_H(1)$ absorption band at $E_L = 1.775$ eV. The exciting laser light is polarized along X ($e_L \| [110]$), the polarization of the scattered light varies in 15° steps between X ($e_S \| [110]$) and Y ($e_S \| [\bar{1}10]$). T = 7 K.

which clearly changes in magnitude from <1 to >1. A quantitative analysis of integrated intensities in the X,X- and X,Y-polarized spectra shows that, turning the analyser around by 90°, the reduction of line intensities is strongest for the $v = 4 \rightarrow 3$ Raman process. It amounts to 85%, while lines $v = 3 \rightarrow 2$, $2 \rightarrow 1$ and $1 \rightarrow 0$ are reduced by about 62, 46 and 30%, respectively. A qualitatively similar behaviour, although less strongly marked, is observed from analysing the intensities in figure 4 for polarization $e_L \| Z$.

To explore these surprising results further, we use a polar coordinate diagram to represent the measured intensities in the X–Y plane as a function of the angle ϕ between the scattered light polarization vector e_S and the X-direction. Figures 6 and 7 show the angular distributions for the Raman lines $v = 3 \rightarrow 2$ and $4 \rightarrow 3$ obtained by $F_H(1)$ excitation with light polarized along X and Z, respectively. These plots not only demonstrate that the intensity distribution is strongly anisotropic and that the anisotropy is markedly different depending on incident light polarization, but even more important we find the symmetry axes of the distributions rotated in the X–Y plane with respect to the crystal symmetry axes X and Y. Consistent with the

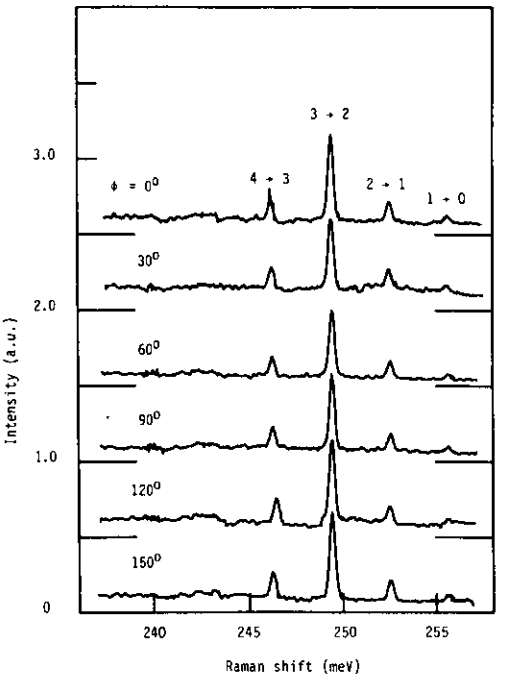

Figure 4. Same as in figure 3, but with the exciting light polarized along Z (e_L||[001]). The polarization of the scattered light varies in 30° steps between X (e_S||[110]) and Y (e_S||[$\bar{1}$10]). T = 7 K.

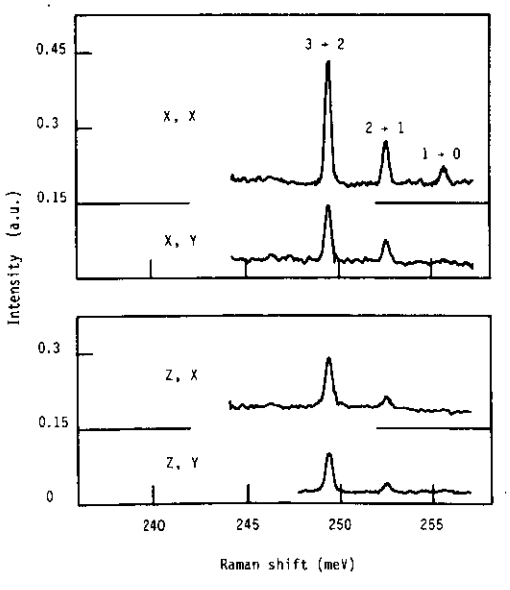

Figure 5. Anti-Stokes resonant Raman spectra excited in the $F_H(2)$ absorption band at E_L = 1.980 eV. The exciting laser light is polarized along X (e_L||[110]) and Z (e_L||[001]), the scattered light along X (e_S||[110]) and Y (e_S||[$\bar{1}$10]) as shown.

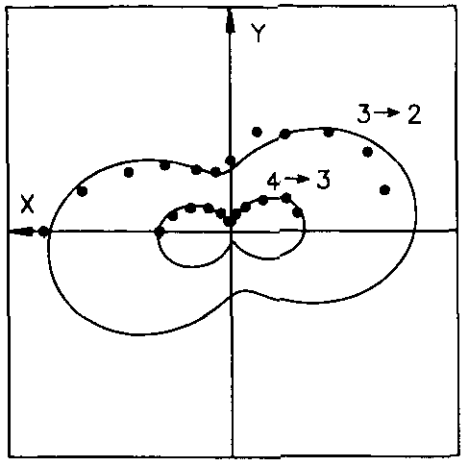

Figure 6. Angular dependence of scattered intensities for two anti-Stokes Raman lines $v = 3 \rightarrow 2$ and $4 \rightarrow 3$ in the X–Y plane. The spectra are excited in the $F_H(1)$ absorption with light polarized along X ($e_L \| [110]$). The experimental data (full points) are shown together with the fit (full lines) according to equation (6).

observations above (see (ii)), the angle of rotation depends on the quantum number v as is most clearly visible from comparing the two angular distributions represented in figure 6.

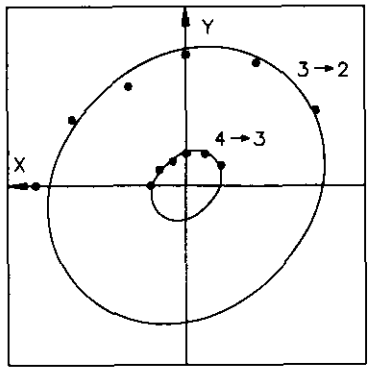

Figure 7. Same as in figure 6, but excited with light polarized along Z ($e_L \| [001]$) and fit according to equation (7).

Although for $F_H(2)$ band excitation the Raman signals are smaller and therefore intensity measurements are less accurate, we find the polarization behaviour in this case qualitatively similar. As for $F_H(1)$ excitation the angular distributions of the signal strength are anisotropic. They are different for $e_L \| X$ and $e_L \| Z$ with their major axes again rotated with respect to the X- and Y- directions.

The angular intensity dependence could in all cases be quantitatively described by the theoretically expected behaviour given below by equations (6) and (7). In order to

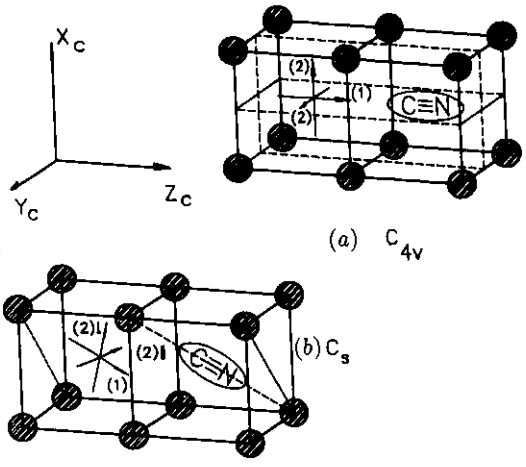

Figure 8. Structural defect models discussed in the text. The CN^- sits on a NNN lattice site relative to the F centre and is oriented along [0 0 1] and $[\bar{1}\,\bar{1}\,1]$, respectively. For the C_{4v} model (*a*) the electronic transition moments of $F_H(1)$ and $F_H(2)$ are oriented along [0 0 1] and [0 1 0],[1 0 0]; for the C_s model (*b*) along $[\bar{1}\,\bar{1}\,1]$ ($F_H(1)$), [1 1 2] ($F_H(2\|)$), and $[1\,\bar{1}\,0]$ ($F_H(2\perp)$). Mirror planes are indicated by dashed lines.

allow later comparison with the predictions of the different structural models, we have summarized in table 1 the (relative) values of the intensity factors for the strongest transition $v = 3 \rightarrow 2$ obtained from fitting the experimental data.

Table 1. Relative intensity factors according to equations (6) and (7) of the $v = 3 \rightarrow 2$ anti-Stokes Raman line obtained from the measured angular dependence (figures 3–7). I and I' are the intensities for $F_H(1)$ and $F_H(2)$ excitation with (X, X)-polarized light ($\phi = 0$).

Excitation	$I_{XX,XX}$	$I_{YX,YX}$	$I_{XX,YZ}$	$I_{XZ,XZ}$	$I_{YZ,YZ}$	$I_{XZ,YZ}$
$F_H(1)$	I	$0.39I$	$0.15I$	$0.35I$	$0.29I$	$0.03I$
$F_H(2)$	I'	$0.52I'$	$0.15I'$	$0.39I'$	$0.33I'$	$0.06I'$

We emphasize at this point that the experimentally observed polarization behaviour is inconsistent with that expected for the previously postulated $F_H(CN^-)$ defect. The structural model of this defect depicted in figure 8 has C_{4v} point symmetry. Owing to the ⟨100⟩ (fourfold) symmetry axis of this model, one would qualitatively expect the scattered intensity distribution to reflect the symmetry of the crystal axis which is clearly not the case in our measurements.

4. Analysis of experimental results and discussion

To compare the measured polarization behaviour in section 3 with model predictions and to substantiate the only qualitative conclusions about the defect symmetry given above, we have performed calculations of scattered intensities. Assuming our experimental scattering geometry, we have examined models of the $F_H(CN^-)$ defect having two different symmetries. One is the usual $F_H(CN^-)$ structure with the

hitherto assumed C_{4v} symmetry. Since no agreement was found between experiment and theory for this structure, we also considered models in which we tentatively assumed deviations of the CN^- molecular axis from the F-centre/CN^- pair axis. These centres possess C_s symmetry.

4.1. Calculation of scattered intensities: principle

Owing to the orientational degeneracy of a low-symmetry defect in a cubic crystal (symmetry O_h for cesium halide structure), the total Raman intensity consists of contributions of all possible defect orientations and may be written as

$$I_{e_L,e_S} = \sum_n N^{(n)} I^{(n)}_{e_L,e_S}. \tag{1}$$

Although this equation holds quite generally for localized defects, in the particular case of the $F_H(CN^-)$ centre the right-hand product quite obviously reflects the fact that light scattering here may be considered to originate from a two-step process (see, e.g., (Cachei *et al* 1989)). In this process, electronic excitation via electronic-vibrational energy transfer results in a distribution of population among the CN^- vibrational states which is subsequently probed by Raman scattering. $I^{(n)}_{e_L,e_S}$ denotes the (polarized) Raman intensity per unit defect concentration contributed by the nth defect orientation. In terms of the corresponding second rank Raman tensor $\mathbf{R}^{(n)}$ and the polarization (unit) vectors e_L and e_S of the incident (laser) and scattered light it is given by

$$I^{(n)}_{e_L,e_S} = cI_0 \left| e_S^{\mathrm{T}} \mathbf{R}^{(n)} e_L \right|^2 \tag{2}$$

where I_0 denotes the excitation intensity, c is an instrumental efficiency factor and the superscript T stands for 'transposed'.

The Raman tensor as available in the literature (Hayes and Loudon 1978) is usually represented for only one particular defect orientation with respect to the surrounding crystal lattice. To obtain the intensity contributions of all other possible (equivalent) orientations n (here always assumed to exist in equal concentration), this tensor ($\mathbf{R}^{(1)}$, say) has to be transformed within the crystal coordinate system X_c, Y_c, Z_c by applying rotations compatible with the (O_h) crystal symmetry. With $\mathbf{B}_n$ denoting an appropriate rotation matrix, one thus may write

$$\mathbf{R}^{(n)} = \mathbf{B}_n \cdot \mathbf{R}^{(1)} \cdot \mathbf{B}_n^{\mathrm{T}}. \tag{3}$$

Another rotation ($\mathbf{B}_c$) has to be applied for each $\mathbf{R}^{(n)}$ to be transformed into the laboratory system (coordinates X, Y, Z) in which the polarization vectors e_L, e_S are defined (see figure 2).

The factor $N^{(n)}$ in equation (1) represents the concentration of vibronically excited defects of orientation n which are produced by the electronic excitation. Assuming the electronic–vibrational energy transfer to be a linear effect, $N^{(n)}$ is directly proportional to the electronic absorption strength. Indeed, it is experimentally verified that the population of the CN^- vibrational levels depends strongly on incident light polarization, i.e. on the spatial orientation of the transition moment. We therefore take

$$N^{(n)} \propto |e_L \cdot M^{(n)}|^2 \tag{4}$$

for each defect orientation n, with $M^{(n)}$ denoting the transition moment in the laboratory frame. It is obtained from the (normalized) components of the

F_H transition moment M_c defined in the crystal reference system X_c, Y_c, Z_c by corresponding rotations into the laboratory system according to

$$M^{(n)} = \mathbf{B}_c M_c^{(n)} = \mathbf{B}_c \mathbf{B}_n M_c^{(1)}. \tag{5}$$

The proportionality constant (omitted in equation (4)) then contains the details of the transfer process and depends on the vibrational quantum number v to account for the non-uniform distribution of population among the vibrational states after termination of the transfer.

According to these considerations, the Raman intensities are calculated by taking the following steps:

(i) Assuming a particular (suspected) defect point symmetry, the Raman tensor component ($\mathbf{R}^{(1)}$) appropriate to the irreducible representation of the CN^- vibrational mode is selected.

(ii) The Raman tensors $\mathbf{R}^{(n)}$ for all n equivalent defect orientations are determined by applying suitable rotations in the crystal reference system X_c, Y_c, Z_c (equation (3)).

(iii) All $\mathbf{R}^{(n)}$ are transformed into the laboratory coordinates X, Y, Z.

(iv) Similarily the components of the F_H transition moment are determined in the X_c, Y_c, Z_c system and transformed into the laboratory reference frame (equation (5)).

(v) From these, the excitation probabilities for each defect orientation are calculated taking into account the incident light polarization (equation (4)).

(vi) Finally, using the result of (iii) and (v), the total scattering intensity is calculated (equation (1)).

This procedure results in the following general expressions for the scattered intensity:

$$I_X(\phi) = I_{XX,XX}\cos^2\phi + I_{YX,YX}\sin^2\phi + I_{XX,YX}\sin 2\phi \tag{6}$$

for excitation $e_L \| X$ and

$$I_Z(\phi) = I_{XZ,XZ}\cos^2\phi + I_{YZ,YZ}\sin^2\phi + I_{XZ,YZ}\sin 2\phi \tag{7}$$

for excitation $e_L \| Z$, where we have introduced the intensity factors

$$I_{\alpha\beta,\gamma\delta} = \sum_n N^{(n)} R_{\alpha\beta}^{(n)} R_{\gamma\delta}^{*(n)}. \tag{8}$$

The angular dependence is completely determined by three parameters for each excitation polarization. $I_{XX,XX}$ and $I_{XZ,XZ}$ represent the intensities of scattered light with $e_S \| X$, $I_{YX,YX}$ and $I_{YZ,YZ}$ the intensity with $e_S \| Y$ for excitation with $e_L \| X$ and $e_L \| Z$, respectively. The quantities $I_{XX,YX}$ and $I_{XZ,YZ}$ measure deviations from the fourfold rotational symmetry.

4.2. Examination of C_{4v} defect symmetry

Applying the formalism outlined in section 4.1, we first examine the structural model of the $F_H(CN^-)$ centre represented in figure 8. Here the F centre and the CN^- molecular ion substitute two NNN anions to form a pair oriented along ⟨100⟩ in the lattice. An important feature of this model is the orientation of the CN^- molecular axis along Z_c, i.e. parallel to the F-centre/CN^- pair axis. This results in the C_{4v} point symmetry of the defect and, disregarding the inversion symmetry of the crystal, in

the threefold orientational degeneracy ($n = 3$) that corresponds to the number of ⟨100⟩ axes. The CN^- stretching vibration (also along Z_c) transforms according to the irreducible representation A_1 (or Γ_1) of this point group. For this case, the Raman tensor component contains only diagonal elements and has the form

$$\mathbf{R}^{(1)} = \begin{pmatrix} a & 0 & 0 \\ 0 & a & 0 \\ 0 & 0 & b \end{pmatrix} \tag{9}$$

with a and b measuring the derivative of the polarizability perpendicular and parallel to the symmetry axis, respectively (Hayes and Loudon 1978).

Compatible with the C_{4v} symmetry and the orientation of the excited F-centre 2p wavefunctions, the $F_H(1)$ and $F_H(2)$ absorption bands (see figure 1) correspond to transitions polarized parallel ($1s \rightarrow 2p_Z$) and perpendicular ($1s \rightarrow 2p_X$, $2p_Y$) to the centre axes (see figure 8). In the defect reference system (unit vectors $e_{X_c}, e_{Y_c}, e_{Z_c}$) the total transition moment is given by

$$M^{(1)} = e_{X_c} M_\perp + e_{Y_c} M_\perp + e_{Z_c} M_\parallel \tag{10}$$

with $M_\perp = 1, M_\parallel = 0$ and $M_\perp = 0, M_\parallel = 1$ for the $F_H(2)$ and $F_H(1)$ transitions, respectively. Here we neglect a mixing of the 2p states of the F centre by spin–orbit interaction. Due to the large energy splitting this effect is small and changes the transition moments by less than 5 per cent (Albrecht 1989).

Taking into account the orientational degeneracy and following the procedure described before, it is straightforward to derive the excitation probabilities. They are listed in table 2 for incident light polarizations along X and Z. From these the intensity factors are then determined. In table 3, they are reproduced in terms of the tensor components which in general depend on the excitation photon energy ($F_H(1)$, $F_H(2)$) and are therefore denoted by a, b and a', b'.

Table 2. Excitation probabilities $N^{(n)} \propto |e_L \cdot M^{(n)}|^2$ calculated for the different defect orientations n of the C_{4v} structural model.

	$F_H(1)$ excitation		$F_H(2)$ excitation	
n	$e_L \| X$	$e_L \| Z$	$e_L \| X$	$e_L \| Z$
1	0	1	1	0
2	$\frac{1}{2}$	0	$\frac{1}{2}$	1
3	$\frac{1}{2}$	0	$\frac{1}{2}$	1

Table 3. Theoretical intensity factors for Raman scattering by A_1 (or Γ_1) vibrations and C_{4v} defect symmetry. The $I_{\alpha\beta,\gamma\delta}$ are given in terms of the corresponding Raman tensor elements (equation (9)) which may be different for $F_H(1)$ and $F_H(2)$ excitation (a, b and a', b', respectively).

Excitation	$I_{XX,XX}$	$I_{YX,YX}$	$I_{XX,YX}$	$I_{XZ,XZ}$	$I_{YZ,YZ}$	$I_{XZ,YZ}$
$F_H(1)$	$\frac{1}{4}(a+b)^2$	$\frac{1}{4}(a-b)^2$	0	0	0	0
$F_H(2)$	$a'^2 + \frac{1}{4}(a'+b')^2$	$\frac{1}{4}(a'-b')^2$	0	0	0	0

Comparison of table 3 with the data listed in table 1 clearly demonstrates that the experimental results are inconsistent with the presumed C_{4v} symmetry of the F-centre/CN^- complex. In particular for the polarization $e_L \| Z$ of the incident laser, no scattering intensity is to be expected, and that both for $F_H(1)$ and $F_H(2)$ excitation. Experimentally, however, in these cases appreciable intensities are found which, we believe, are much too strong to be explained by any experimental insufficiency. We have especially convinced ourselves that sample misorientation cannot account for the intensities actually observed. Assuming a deviation from the crystal axis (X or Y) as large as 5°, the intensities for $e \| Z$ would in fact be smaller by a factor of 35 than those found experimentally. Further clear evidence, that inadequate experimental conditions must be ruled out as source for the disagreement is the observed dependence of Raman intensities on scattered light polarization $I_{X,Z}(\phi)$ which, for fixed e_L, turned out different depending on vibrational quantum number v (see section 3 (ii)). In addition, the calculated intensity factors $I_{XX,YX}$ and $I_{XZ,YZ}$ are identically zero, which is expected for the fourfold rotational symmetry of C_{4v}, but is distinctly different from the experimental findings.

4.3. Possible models with C_s symmetry

The disagreement between the measured Raman intensities and the C_{4v} structural model led us to examine a number of other possible defect configurations. In CsBr the CN^- molecular ion, if not perturbed by a nearby defect, is known to orient in the lattice along ⟨111⟩ (von der Osten and Lüty 1987, Cachei 1990). We therefore tested especially the structure displayed in figure 8(*b*) assuming that no reorientation of the molecule had occurred during aggregation with the F centre. The only symmetry element of this model is a $(\bar{1}10)$ mirror plane which contains the F-centre/CN^- axis (along Z_c). The F-centre transition moments need to be specified relative to this plane. Assuming the $F_H(1)$ transition to have a moment parallel to the CN^- molecular axis (in figure 8(*a*) parallel $[\bar{1}\bar{1}1]$), the two $F_H(2)$ moments are no longer equivalent and, hence, the transitions may be non-degenerate. The moments are oriented along [112] and $[1\bar{1}0]$, respectively, lying within the mirror plane ('$F_H(2\|)$') and perpendicular to it ('$F_H(2\perp)$'). This structural model has C_s point symmetry with $n = 12$ equivalent orientations in the crystal. In contrast to the C_{4v} model, in the electronic ground state of this centre several equivalent CN^- orientations exist between which, in principle, tunnelling motion is possible. In figure 8, this tunnelling would correspond to a rotation around the Z_c axis but, to a first approximation, it will be neglected. In this case, due to the low symmetry, the Raman tensor for the CN^- stretching vibration is of the form

$$\mathbf{R}^{(1)} = \begin{pmatrix} a & 0 & d \\ 0 & b & 0 \\ e & 0 & c \end{pmatrix}. \tag{11}$$

It has both diagonal and off-diagonal elements and in case of resonant scattering is non-symmetric ($d \neq e$). As before (table 3), we have calculated the intensity factors as functions of the Raman tensor elements for the different excitation conditions. Of these, only the results for the clearest case of $F_H(1)$ excitation are reproduced in table 4. Compared with the calculation for the C_{4v} centre (table 3) two differences arise. Most important is that the calculation gives non-zero and equal components $I_{XZ,XZ}$ and $I_{YZ,YZ}$ for excitation with $e_L \| Z$. Furthermore, it predicts a strong anisotropic component $I_{XX,YX}$ for X excitation, but a vanishing anisotropy

$I_{XZ,YZ}$ in the case of Z excitation. All these predictions are in good qualitative agreement with the experimental results from table 1. The small deviations may be due to experimental uncertainty. They would also be explainable by an additional reorientation process, e.g. a tunnelling motion of the CN^- molecule between the different equivalent orientations, which we neglected in the calculations. As this mixes the two cases of excitation polarization, any CN^- reorientation would explain the deviations found experimentally. Here further experiments, particular in connection with time-resolving techniques, are necessary.

Table 4. Intensity factors for Raman scattering by A_1 (or Γ_1) vibrations and C_s defect symmetry for $F_H(1)$ excitation. The relation between the intensity factors and the Raman tensor elements a, b, c, d and e as given in the last three rows are different for the three possible orientations of the CN^- long axis.

Orientation of CN^-	$I_{XX,XX}$ $\frac{1}{3}(\alpha+\beta)$	$I_{YX,YX}$ $\frac{1}{3}(\alpha-\beta)$	$I_{XX,YX}$ $\frac{1}{3}\delta$	$I_{XZ,XZ}$ $\frac{1}{3}\gamma$	$I_{YZ,YZ}$ $\frac{1}{3}\gamma$	$I_{XZ,YZ}$ 0
[111]	$\alpha=(a^2+c^2)/2+2(a^2+b^2)+d^2+e^2+ac$ $\beta=2(a^2+ab+cb+de)$ $\gamma=(a-c)^2+2(d^2+e^2)$ $\delta=\sqrt{2}(2eb-ad-cd)$					
[110]	$\alpha=(a^2+c^2)/2+2b^2+d^2+e^2+ac$ $\beta=2(ab+cb+de)$ $\gamma=(a-c)^2+2e^2$ $\delta=\frac{1}{\sqrt{2}}(2eb-ad-cd)$					
[100]	$\alpha=(a^2+c^2)/2+2(a^2+b^2)+d^2+e^2+ac$ $\beta=2(a^2+ab+cb+de)$ $\gamma=3e^2$ $\delta=\frac{3}{2}(eb-ad)$					

Despite the improvement in explaining the Raman data, a definite conclusion on the structural model cannot be drawn as there exist other orientations of the CN^- molecule which also possess C_s symmetry. In these, the long axis of the CN^- is oriented either along a ⟨110⟩ or a ⟨100⟩ direction, but each is perpendicular to the F-centre/CN^- - axis. The intensity factors for these structures can be cast into the same closed form as those for the ⟨111⟩ centre, but with a different functional dependence on the Raman tensor elements, as also given in table 4.

The Raman measurements unfortunately do not provide sufficient information to distinguish between the different possibilities. This is because a defect of such low symmetry, due to contributions from a large number of orientationally degenerate centres (here $n = 12$), does not result in very significant differences between differently polarized Raman intensity components, thus making an unambiguous identification difficult. In particular, quantitative calculations of the (relative) intensities are impossible because the magnitude of the relevant tensor elements are unknown.

We also do not observe an additional splitting of the $F_H(2)$ band (except a weak absorption shoulder of so far unknown origin at 2.1 eV; cf figure 1) which would be implied by the non-equivalence of the two $F_H(2)$ transition moments and certainly would support the model. However, this splitting may not be resolvable due the additional effect of spin–orbit interaction, which has to be taken into account for a full quantitative analysis.

In addition, using the same assumptions, we calculated the polarized intensities of the infrared vibrational emission for all models (Albrecht 1989), but in no case found them to agree satisfactorily with the available experimental data (Yang *et al* 1985).

5. Concluding remarks

It is clear from sections 3 and 4 that the experimental Raman results are inconsistent with the calculations based on the C_{4v} point symmetry assumed for the F-centre/CN^- defect complex. The disagreement shows up most clearly in the observed asymmetric angular dependence of the scattered intensity and in the strong Raman signals found in forbidden polarizations. In retrospect, similar strong deviations from the behaviour expected for the C_{4v} model also occurred in polarized infrared vibrational emission in CsCl (Yang *et al* 1985). In spite of the fact that the above model with C_s point symmetry seems to improve the agreement, a definite conclusion on the microscopic centre structure cannot be drawn. To explain our results completely, in particular one might have to take into consideration dynamical reorientation effects of the CN^- molecular ion. In the present case of resonant Raman scattering, these may occur instantaneously during the electronic excitation process. Also, they could take place after the electron has already returned to the ground state while the CN^- is left behind in a highly excited vibrational state. Since equation (4) for the excitation probability does not account for any of these effects, it is evident that the selection rules which have been used to derive the intensities would not be applicable. Further experimental work to explore the possibility of dynamical reorientation effects is under way.

Acknowledgments

We wish to thank Professor B Lendermann of the Chemistry Department, Universität Paderborn, for kindly synthesising the doping material. We also appreciate financial support from the Deutsche Forschungsgemeinschaft.

References

Albrecht R 1989 *Diplomarbeit* Universität Paderborn
Cachei G, Stolz H, von der Osten W and Lüty F 1989 *J. Phys.: Condens. Matter* **1** 3239
Cachei G 1990 unpublished
DeLong M C and Rosenberger F 1986 *J. Cryst. Growth* **75** 164
Hayes W and Loudon 1978 *Scattering of Light by Crystals* (New York: Wiley)
Jordan M, Söthe H, Spaeth J M and Lüty F 1988 *Proc. Int. Conf. Defects in Insulating Crystals, (Parma 1988)* p 11
Lüty F 1968 *Physics of Color Centers* ed W B Fowler (New York: Academic) p 181
von der Osten W and Lüty F 1987 *Phys. Rev.* B **35** 7684
Rong F, Yang Y and Lüty F 1989 *Cryst. Latt. Def. Amorph. Mat.* **18** 1
Yang Y, von der Osten W and Lüty F 1985 *Phys. Rev.* B **32** 2724